

---

# A Comparative Analysis of Radial-Tchebichef Moments and Zernike Moments

Ramakrishnan Mukundan  
<http://www.cosc.canterbury.ac.nz/>

Department of Computer Science  
and Software Engineering  
University of Canterbury,  
Christchurch, New Zealand

---

## Abstract

Orthogonal moment descriptors are commonly used in applications such as image classification, pattern recognition and identification. A radial-polar representation of image coordinate space is particularly useful in the above applications, since it facilitates the derivation of rotation invariants of any arbitrary order. Zernike moments and radial-Tchebichef moments fall into the category of moments that are defined using radial-polar coordinates. The discrete orthogonal nature of the kernel of radial-Tchebichef moments provides notable advantages over continuous Zernike moments. The paper presents a detailed analysis to prove that radial-Tchebichef moments have superior features compared to Zernike moments and are computationally less complex. The paper also introduces a novel and fast method for accurate computation of radial moments, preserving rotation-invariant characteristics. The efficiency of the proposed method is demonstrated through a series of experimental results.

## 1 Introduction

Rotation invariant moment functions play a very important role in many image analysis applications such as pattern and character recognition [1], object identification[2], template matching and texture classification[3]. While feature descriptors that are invariant with respect to translation and scale transformation can be obtained relatively easily, the construction of rotation invariants requires more complex mathematical structures that can isolate the effects of image rotation. Teague [4] introduced the general theory of orthogonal invariants based on Zernike polynomials using which rotation invariants of arbitrary order could be constructed.

The primary advantages Zernike moments have over other types of moments are their orthogonality and robustness [5]. Zernike polynomials are orthogonal only in the continuous domain of the interior of a unit circle. Computing Zernike moments also requires mapping of radial distances to the range  $[-1, 1]$ , and numerical approximation of the continuous moment integrals [6]. A few types of discrete orthogonal moments have been recently introduced in the field of image analysis, with the aim of improving the feature representation capability and minimizing information redundancy in a moment set. Tchebichef moments [7], Krawtchouk moments [8], and Hahn moments [9] use discrete orthogonal functions for defining two-dimensional rectangular image moments.

Radial-Tchebichef moments [10] can be thought of as a variant of Tchebichef moments, where a definition similar to that of Zernike moments is used to combine one-dimensional Tchebichef polynomials of radial distances with circular functions to form a new class of two-dimensional discrete orthogonal moments. As in the case of Zernike moments, the radial-polar nature of the definition allows us to construct rotation invariants of Tchebichef moments quickly. However, radial-Tchebichef moments use a simpler moment kernel compared to Zernike moments, giving significant reduction in computational overheads. The discrete orthogonality property of radial-Tchebichef moments eliminates the need for transforming the coordinates to a unit circle or using numerical methods for evaluating continuous integrals. In order to exploit this property effectively, we would still need to map the image coordinates to discrete polar coordinates. Even though several solutions to this problem have been proposed in the literature [11],[12], they are primarily useful only for computing continuous moments such as Zernike invariants.

This paper presents a novel framework for accurately computing moments with kernel defined using polar coordinates, that is particularly suitable for discrete orthogonal rotation invariants. The method preserves the separability property of the kernel, which can be effectively used in computing both forward and inverse moment transforms. Thus the proposed framework yields a simple and fast implementation of radial-Tchebichef moments for image reconstruction, and invariants for pattern recognition.

## 2 Radial-Tchebichef Moments

The basis functions of Radial-Tchebichef moments [10] are products of one-dimensional Tchebichef polynomials [7] in radial distance  $r$  and circular functions of the angle  $\theta$ . For a given image of size  $N \times N$ , we require a discrete domain for these functions. The most appropriate mathematical structure for computing radial Tchebichef moments is a set of discrete concentric rings, where each ring represents a fixed integer value of radial distance  $r$  from the centre of the image. We can subdivide the coordinate space into  $N/2$

concentric rings  $R_r$ ,  $r = 0, 1, \dots, (N/2)-1$ . Depending on the number of points inside a ring, each ring can be further subdivided into  $m_r$  regions. An example for  $N = 10$  is shown in Figure 1(a).

On ring  $R_r$ , the angle  $\theta$  varies from 0 to  $2\pi$  in  $m_r$  discrete intervals such that

$$\theta_k = \frac{2\pi k}{m_r}, \quad k = 0, 1, 2, \dots, m_r-1. \quad (1)$$

Eq. (1) is valid only under the assumption that there exists a one-to-one mapping between pixels on the image, and points that are distributed uniformly around concentric circles. This mapping and the computation of  $m_r$  will be discussed in next section. If we denote the image intensity value at location  $(r, \theta_k)$  by  $f(r, k)$ , then the radial-Tchebichef moments of order  $p$  and repetition  $q$  are defined using the equation

$$T_{pq} = \sum_{r=0}^{N/2-1} t_p(r) \sum_{k=0}^{m_r-1} \frac{1}{m_r} e^{-j \frac{2\pi qk}{m_r}} f(r, k), \quad p = 0, 1, \dots, (N/2)-1, \quad q = 0, 1, \dots, m_r-1. \quad (2)$$

If an image is rotated about the origin ( $r=0$ ) by an angle  $\phi$ , and if the intensity values are preserved during rotation, then the moments  $T_{pq}$  should ideally get transformed to  $T'_{pq}$  such that

$$T'_{pq} = T_{pq} e^{-jq\phi} \quad (3)$$

If we write  $T_{pq}$  in terms of its real and imaginary parts as  $T_{pq} = C_{pq} - j S_{pq}$ , we can remove the effects of rotation  $\phi$  by constructing the following types of invariants:

$$\begin{aligned} \text{Type 1: } I_{p0} &= C_{p0} \\ \text{Type 2: } I_{pq} &= \sqrt{C_{pq}^2 + S_{pq}^2} \end{aligned} \quad (4)$$

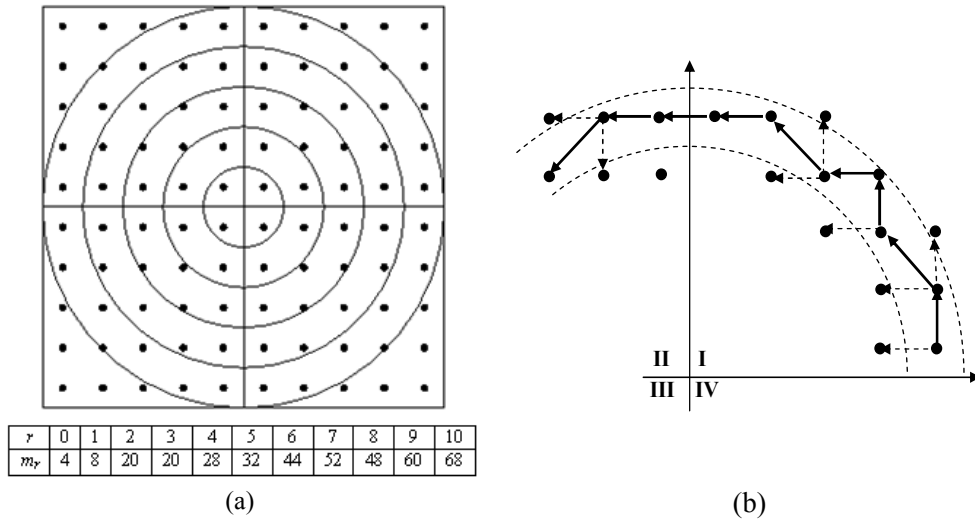


Figure 1: (a) A 10x10 pixel space subdivided into 5 concentric rings  $R_0..R_4$ . The middle ring  $R_0$  contains 4 pixels whereas the ring  $R_4$  contains 28 pixels. (b) The ring traversal algorithm for ring  $R_4$  starts with the lowermost point within the ring in the first quadrant, and incrementally visits all the remaining points in the ring. The arrows point to the candidate pixels at each iteration, and the solid arrow points to the next selected pixel.

### 3 The Ring Structure

In the previous section, we observed that the evaluation of radial-Tchebichef moments requires a mapping from Cartesian coordinates  $(x, y)$  to discrete polar coordinates  $(r, \theta_k)$ . If a pixel has image coordinates  $(x, y)$ ,  $x, y = 0, 1, \dots, N-1$ , then we transfer its coordinates to the centre of the image as  $(u, v)$  where

$$u = x - (N/2) + 0.5; \quad v = y - (N/2) + 0.5 \quad (5)$$

The point  $(x, y)$  then belongs to the ring  $R_r$  where  $r$  is given by

$$r = \text{trunc} \left( \sqrt{u^2 + v^2} \right) \quad (6)$$

The method described below gets the list of all points (pixels) on each ring using incremental updates, and works similar to rasterization algorithms for circle drawing. For each value of  $r = 0, \dots, (N/2)-1$ , the algorithm starts with the first point on the ring  $R_r$ , whose image coordinates are given by

$$x = r + (N/2); \quad y = N/2. \quad (7)$$

This point has the minimum value of  $\theta$  on ring  $R_r$ . We define two orthogonal unit vectors  $(d_x, d_y)$ , and  $(e_x, e_y)$ , and select three

candidate pixels at the current location as follows:

$$\begin{aligned} x_1 &= x + d_x; & y_1 &= y + d_y; \\ x_2 &= x + e_x; & y_2 &= y + e_y; \\ x_3 &= x + d_x + e_x; & y_3 &= y + d_y + e_y \end{aligned} \quad (8)$$

The values of the unit vectors for each quadrant are given below (see Figure 2).

$$\begin{aligned} \text{Quadrant I:} & & (d_x, d_y) &= (-1, 0), & (e_x, e_y) &= (0, 1) \\ \text{Quadrant II:} & & (d_x, d_y) &= (-1, 0), & (e_x, e_y) &= (0, -1) \\ \text{Quadrant III:} & & (d_x, d_y) &= (1, 0), & (e_x, e_y) &= (0, -1) \\ \text{Quadrant IV:} & & (d_x, d_y) &= (1, 0), & (e_x, e_y) &= (0, 1) \end{aligned} \quad (9)$$

Among the three candidate pixels  $(x_1, y_1)$ ,  $(x_2, y_2)$ ,  $(x_3, y_3)$ , we choose the pixel that lies within the ring as the next point, and the iteration continues with this point. This process, which we call the ring traversal algorithm, will automatically visit all points within the ring in the ascending order of the angle  $\theta$ . The process is illustrated in Figure 1(b), using ring  $R_4$  from Figure 1(a) as an example.

The algorithm described above is very efficient in that it visits each pixel in the image exactly once, and yields a one-to-one mapping of Cartesian coordinates of pixels to radial-polar coordinates. If  $m_r$  denotes the number of pixels on ring  $R_r$ , we can calculate the following one-dimensional moments using circular functions for each  $r$ :

$$\begin{aligned} \alpha_q(r) &= \frac{1}{m_r} \sum_{k=0}^{m_r-1} \cos\left(\frac{2\pi q k}{m_r}\right) f(r, k) \\ \beta_q(r) &= \frac{1}{m_r} \sum_{k=0}^{m_r-1} \sin\left(\frac{2\pi q k}{m_r}\right) f(r, k), \quad r = 0, 1, \dots, N/2-1; \quad q = 0, 1, 2, \dots, m_r-1. \end{aligned} \quad (10)$$

Both the above functions are periodic in  $q$ , and satisfy the following properties, for  $r = 0, 1, \dots, N/2-1$ :

$$\begin{aligned} \alpha_{q+m_r}(r) &= \alpha_q(r); & \beta_{q+m_r}(r) &= \beta_q(r), \\ \alpha_{-q}(r) &= \alpha_q(r); & \beta_{-q}(r) &= -\beta_q(r), & \beta_0(r) &= 0. \end{aligned} \quad (11)$$

Therefore, for a given  $r$ , the value of  $q$  need be varied from 0 to  $m_r-1$  only. This result yields an efficient procedure for the computation of radial-Tchebichef invariants as detailed below:

Given a pair of values  $p$  and  $q$ , the values of  $\alpha_q(r)$ ,  $\beta_q(r)$  are computed for each ring  $R_r$  for values of  $q$  varying from 0 to  $m_r-1$  only, with the remaining values computed using the modulo function. The real-valued components of  $T_{pq}$  in (4) are given by

$$C_{pq} = \sum_{r=0}^{N/2-1} \alpha_q(r) t_p(r); \quad S_{pq} = \sum_{r=0}^{N/2-1} \beta_q(r) t_p(r) \quad (12)$$

The above procedure clearly makes use of the separability property, and could be used in conjunction with fast algorithms designed for computing moments. The functions  $C_{pq}$ ,  $S_{pq}$  in (4) are also periodic in  $q$ , and satisfy conditions similar to (11).

The process of image reconstruction could be conveniently split into three stages. In the first stage, we reconstruct the functions  $\alpha_q(r)$ ,  $\beta_q(r)$  using only radial Tchebichef polynomials  $t_p(r)$  of up to a maximum order  $p_{\max}$ :

$$\alpha_q(r) = \sum_{p=0}^{p_{\max}} t_p(r) C_{pq}, \quad \beta_q(r) = \sum_{p=0}^{p_{\max}} t_p(r) S_{pq}, \quad r = 0, 1, \dots, N/2-1; \quad q = 0, 1, 2, \dots, m_r-1. \quad (13)$$

In the second stage, we reconstruct the intensity values at integer-polar coordinates  $(r, k)$ :


$$f(r, k) = \alpha_0(r) + 2 \sum_{q=1}^{m_r/2} \left( \alpha_q(r) \cos \frac{2\pi q k}{m_r} + \beta_q(r) \sin \frac{2\pi q k}{m_r} \right) \quad (14)$$

In the third stage, the integer polar coordinates  $(r, k)$  are mapped back to original pixel coordinates  $(i, j)$ . The separability of the inverse moment transform of radial-Tchebichef moments as shown above, helps in reducing the computational complexity from  $O(N^4)$  to  $O(N^3)$ . The symmetry properties of Tchebichef polynomials [7] and circular moments (10) could be used to further reduce the amount of computations in both moment equations and inverse transforms.

## 4 Experimental Results

The method proposed in the previous section was implemented and tested with a series of images generated using rotational transformations. For the analysis of invariant characteristics of Zernike and radial-Tchebichef moments, three different types of images were used: (i) a binary image of the character ‘‘K’’ of size 256x256 pixels, (ii) a binary image ‘‘Athena’’ of size 120x120 pixels, and (iii) a gray-level image ‘‘Tool’’ of size 120-x120 pixels. The values of four invariant moments for different images are given in Table 1. The standard deviation of the invariants was computed from a set of 360 values obtained for every one degree change in the rotation angle as in Figure 2(a).

The values of Zernike moments tend to become very small as the moment order increases. Radial-Tchebichef moments showed consistently good invariant characteristics for high-order moments ( $p, q > 4$ ). The analysis of rotation invariance of computed moments was repeated by adding 2% salt-pepper noise to the rotated images. The plots of invariants  $I_{53}$  (see Eq. (4)) computed using radial-Tchebichef moments and Zernike moments for the binary image ‘‘K’’ are given in Figure 2(a). The dotted lines in the figures represent the values computed for the noisy image.



Angle	Inv	Rad-Tch	Zernike	Rad-Tch	Zernike	Rad-Tch	Zernike
0 degs	$I_{20}$	2.0128	-0.1489	-0.9739	-0.3204	218.1282	-20.299
	$I_{60}$	0.4445	-0.1192	-0.3522	0.3597	28.9108	-14.151
	$I_{11}$	0.3462	0.0068	0.5638	0.0277	57.5770	1.6775
	$I_{53}$	0.4030	0.0056	0.0937	0.0408	9.6062	2.7494
<b>Std.Dev</b> <b>(<math>\sigma</math>)</b>	$I_{20}$	0.0038	0.0001	0.0102	0.0012	0.9251	0.0888
	$I_{60}$	0.0034	0.0011	0.0090	0.0042	0.7445	0.2400
	$I_{11}$	0.0031	0.0003	0.0079	0.0028	0.5247	0.1042
	$I_{53}$	0.0016	0.0001	0.0044	0.0024	0.4260	0.2167
<b>(<math>\sigma/\mu</math>)*100</b>	$I_{20}$	0.1902	0.1192	1.0439	0.3889	0.4244	0.4372
	$I_{60}$	0.7578	0.8536	2.5841	1.1795	2.5846	1.6794
	$I_{11}$	0.8974	4.5816	1.4308	8.6688	0.9139	6.1433
	$I_{53}$	0.3967	1.6901	4.8605	5.7457	4.4921	7.9038

Table 1: A comparison of rotation invariants of Radial-Tchebichef and Zernike moments.

We have seen that radial-Tchebichef moments could be computed in a separable manner using one-dimensional summations given in (10), (12). Zernike polynomials, on the other hand are two-dimensional functions that require a lot more computations. Figure 2(b) shows the variation of CPU time with moment order for Zernike and radial-Tchebichef moments of a 256x256 gray-level image, as obtained on a 2.8GHz processor with 1GB RAM.

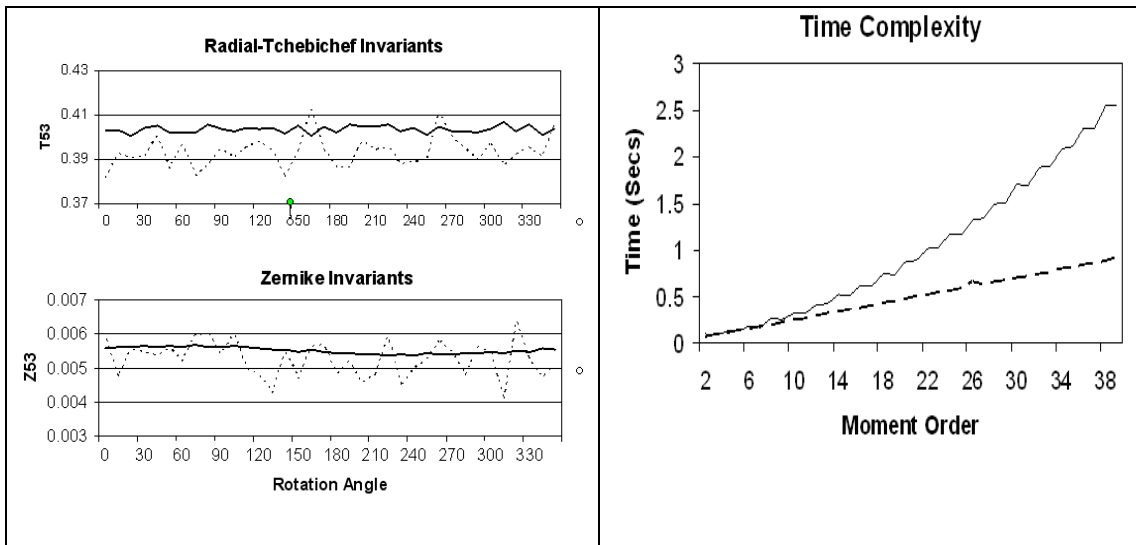


Figure 2: (a) Effects of image noise on Radial-Tchebichef invariants and Zernike invariants ( $I_{53}$ ). The solid line gives the plot of invariants without noise, and the dotted line gives the values computed using the noisy image. (b) Computational complexity of Zernike and radial-Tchebichef moments. The solid line gives the complexity of Zernike moments, while the dotted line gives the complexity of Radial-Tchebichef moments.

Radial-Tchebichef moments provide the same computational advantage over Zernike moments while using the inverse transform for image reconstruction. The reconstruction accuracy of radial-Tchebichef moments was analysed using both binary (Figure 3) and gray-level images (Figure 4). The moment values were computed using (12), and images reconstructed for various values of  $p_{max}$ , using (14). The ring traversal algorithm (Section 3) gave very good reconstructions, owing to the one-one correspondence between pixel values and the intensity values along each circular ring.

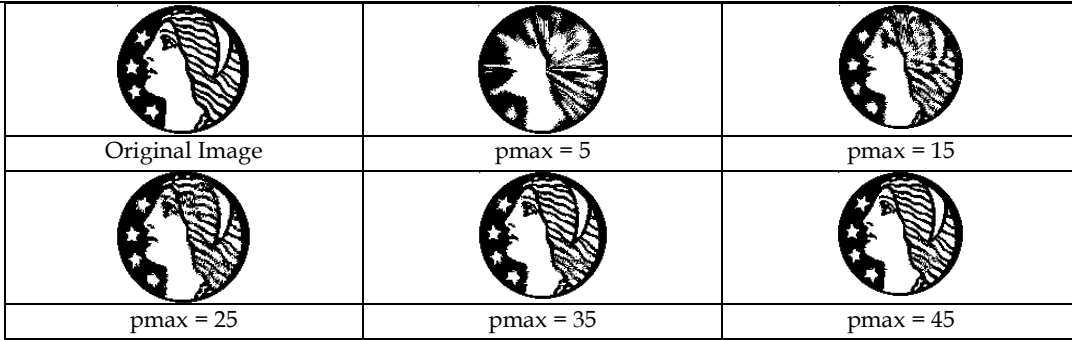


Figure 3: Reconstructions of “Athena” image using radial-Tchebichef moments up to order pmax.

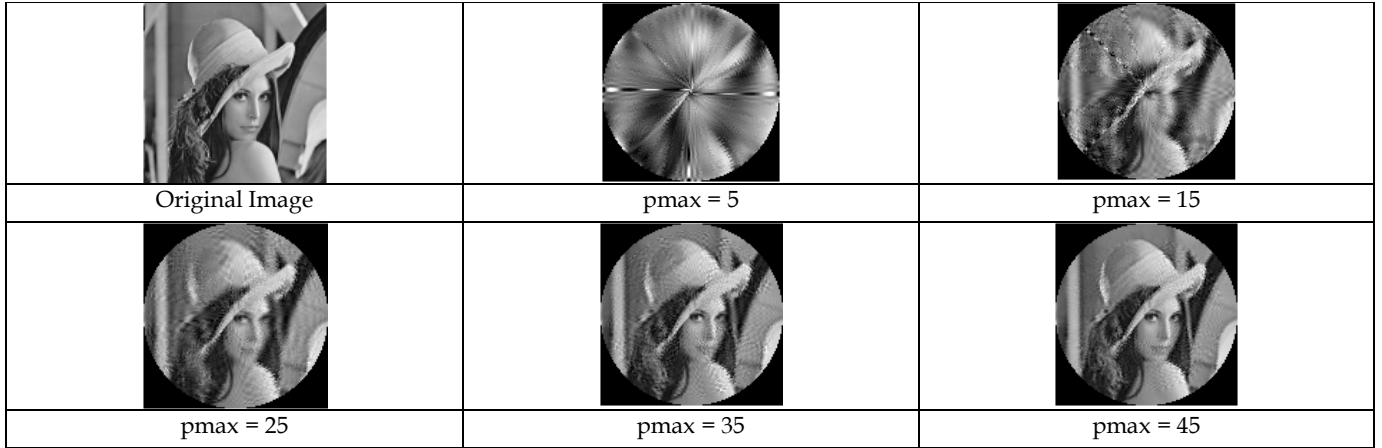


Figure 4: Reconstructions of a 128x128 image “Lenna” using radial-Tchebichef moments up to order pmax.

Zernike moments have relatively fewer number of components for each moment order (see Table 2), and the reconstruction error is correspondingly higher. Various stages of reconstructions of image “Lenna” using Zernike moments are shown in Figure 5. A comparison of the magnitudes and variations of reconstruction errors with moment order given in Figures 6(a), 6(b) clearly show the superior feature representation capability of radial-Tchebichef moments over Zernike moments.

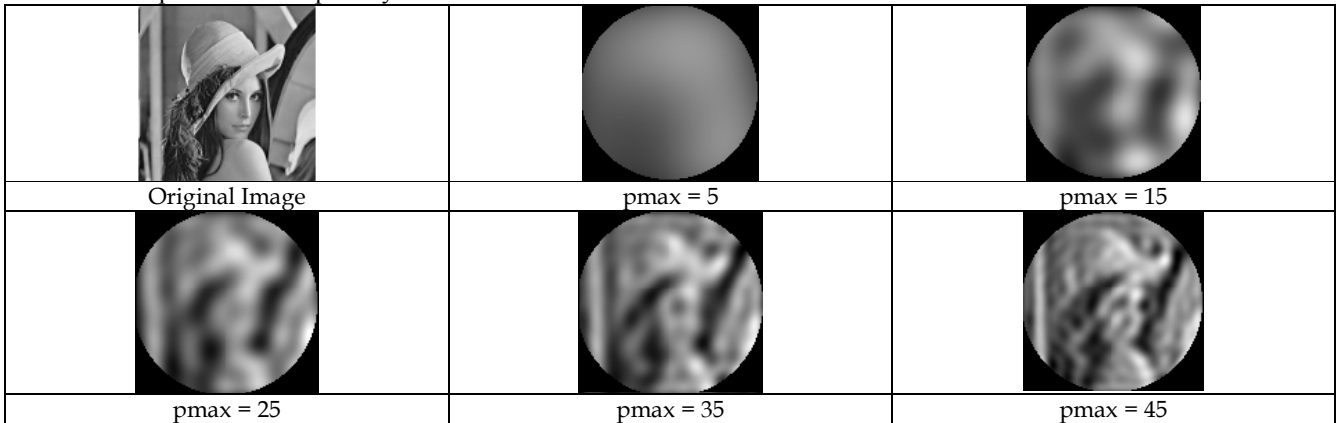


Figure 5: Reconstructions of a 128x128 image “Lenna” using Zernike moments up to order pmax.

The reconstruction error for the gray-level image in Figure 6(a) was computed as the average of squared differences:

$$\varepsilon_1 = \sqrt{\frac{\sum_{x=0}^{N-1} \sum_{y=0}^{N-1} \{f(x, y) - g(x, y)\}^2}{N^2}} \tag{15}$$

whereas, for the binary image reconstruction in Figure 6(b), we used the sum of absolute differences as the error metric:

$$\varepsilon_2 = \sum_{x=0}^{N-1} \sum_{y=0}^{N-1} |f(x, y) - g(x, y)| \tag{16}$$

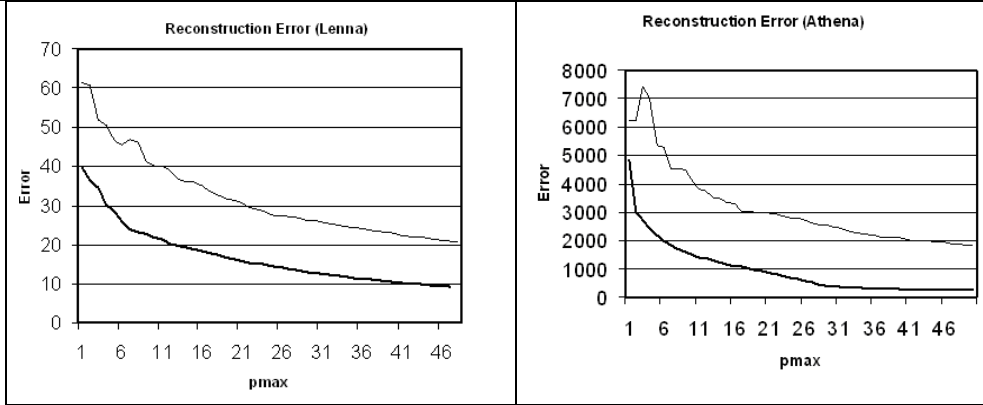


Figure 6: Plot of reconstruction errors with respect to moment order, (a) for the gray-level image “Lenna” and (b) for the binary image “Athena”. The thin line on the top is obtained using Zernike moments, and the thick line using Radial-Tchebichef moments.

	Zernike Moments	Radial-Tchebichef Moments
Kernel function	Continuous, orthogonal	Discrete, orthogonal
Domain of definition	Unit circle $r \in [0,1)$	Image space $r \in [0, N/2)$
Radial polynomial	Two dimensional: $R_m(r)$	One dimensional: $T_p(r)$
Radial polynomial computation	Two-stage recurrence	Simple recurrence
Inverse transform	Non-separable	Separable
Moments of order $p$	$p+1$	$m_r$
Range of values of $q$	Depends on $p$	Independent of $p$

Table 2: Differences in primary characteristics of Zernike and Radial-Tchebichef moments

Table 2 given above summarizes the important differences in the functional characteristics of Zernike and radial-Tchebichef moments. These differences clearly point to the computational advantage radial-Tchebichef invariants have over Zernike invariants.

## 5 Conclusion

This paper has looked at the invariant characteristics of radial-Tchebichef moments, and compared them with that of Zernike moments. Experimental analysis has confirmed that radial-Tchebichef invariants have robust feature representation capability, and notable advantages over Zernike moments. The discrete orthogonal nature of the kernel functions can be utilized to eliminate sources of numerical error present in the computation of their continuous counterparts such as Zernike and Pseudo-Zernike moments. Radial-Tchebichef moments have a simpler functional representation that allows the use of separability property for fast computation of invariants and inverse moment transforms. Radial-Tchebichef moments give better reconstructions and high-order rotational invariants compared to Zernike moments.

This paper has also presented a novel and efficient method for establishing the correspondence between image pixel coordinates and integer-polar coordinates defined along uniformly distributed points along concentric rings. The ring traversal algorithm could be effectively used for computation of invariants and image reconstructions from orthogonal moments. Experimental results were also presented to show a comparison of both the invariance and orthogonality properties of radial-Tchebichef moments and Zernike moments.

The framework presented in the paper shows that radial-Tchebichef moments could be used in practically all situations where Zernike moments are currently used, with the possibility of getting significant performance benefits. Future work in this research is directed towards analyzing the requirements of such applications and looking at more detailed implementation aspects and statistical properties of radial-Tchebichef moments and invariants.

## References

- [1] C. Kan, M.D. Srinath, Invariant character recognition with Zernike and orthogonal Fourier-Mellin moments, Pattern Recognition, 35(1): 143-154, 2002.
- [2] C. Gope, N. Kehtarnavaz, An affine invariant curve matching method for photo-identification of marine mammals, Pattern Recognition, 38(1):125-132, 2005.

- [3] M. Wang, A. Knoesen, Rotation and scale invariant texture features based on spectral moment invariants, *Jnl. Opt. Soc. Of Am. (A)*, 24(9):2550-2557, 2007.
- [4] M. R. Teague, Image analysis via the general theory of moments, *J. Optical Soc. Of America*, 70: 920-930, 1980.
- [5] A. Khotanzad, Invariant image recognition by Zernike moments, *IEEE Trans. Pattern Analysis and Machine Intelligence*, 12(5): 489-497, 1990.
- [6] R. Mukundan, K. R. Ramakrishnan, *Moment Functions in Image Analysis – Theory and Applications*, World Scientific, 1998.
- [7] R. Mukundan, S.H. Ong, P.A. Lee, Image analysis by Tchebichef moments, *IEEE Trans. on Image Processing*, 10(9): 1357-1364, 2001.
- [8] P.T. Yap, R. Paramesran, S.H. Ong, Image analysis by Krawtchouk moments, *IEEE Trans. Image Processing*, 12(11): 1357-1364, 2003.
- [9] J. Zhou et. al., Image analysis by discrete Hahn moments, *Proc. Intl. Conf. on Image Analysis and Recognition (ICIAR)*, 524-531, 2005.
- [10] R. Mukundan, Radial Tchebichef invariants for pattern recognition, *Proc. of IEEE Tencon Conference – TENCON05*, 2098-2103, 2005.
- [11] Y. Xin, S. Liao, M. Pawlak, On the improvement of rotational invariance of Zernike moments, *Proc. IEEE Intl. Conf. on Image Processing (ICIP)*, 2: 842-845, 2005.
- [12] S.X.Liao, M. Pawlak, On the accuracy of Zernike moments for image analysis, *IEEE Trans. Patt. Anal. Mach. Intell.*, 20(12): 1358-1364, 1998.